Open access • Proceedings Article • DOI:10.1109/MED.2014.6961567

Suspended load motion control using multicopters — Source link

Kristian Klausen, Thor I. Fossen, Tor Arne Johansen

Institutions: Norwegian University of Science and Technology

Published on: 16 Jun 2014 - Mediterranean Conference on Control and Automation

Topics: Kinematics and Motion control

Suspended Load Motion Control using Multicopters

Kristian Klausen*, Thor I. Fossen†, Tor Arne Johansen‡
Centre for Autonomous Marine Operations and Systems (AMOS)
Department of Engineering Cybernetics, Norwegian University of Science and Technology,
Email: *kristian.klausen@itk.ntnu.no, †thor.fossen@itk.ntnu.no, ‡tor.arne.johansen@itk.ntnu.no

***Abstract*—This paper presents a distributed kinematic control law for group coordination for several multicopters and a payload suspended with wires from each multicopter. The complete system with constraints on the wires are modeled in 6 degrees of freedom (DOF), using the Udwadia-Kalaba equation. Velocity controllers for the multicopters are developed to realize the desired motion set by the kinematic controller. This results in a system where the group of multicopters are able to maneuver the payload to a desired position while keeping a desired formation. The results are verified by simulations.**

I. Introduction

In many years, especially in the military, a lot of research has been done on modelling and control of a system consisting of flying vehicles transporting a payload suspended with ropes. Helicopters and other multi-rotors are particularly useful for this task due to their hovering ability. Applications span from crate transportation and fire extinguishing, to geo-surveying and mine-detection [1].

Compared to a single multi-copter, several multi-copters with a common lifting arrangement (e.g. lines) provides significantly more stability and some added flexibility to position the spatially distributed lifting arrangement in space and attitude. For example, for rendezvous with objects in order to recover and move them, the end effector could be more stably positioned (less swinging due to e.g. winds) and the end effector could also be a horizontally arranged line segment that would be much easier to hook up with the object to be recovered than a point-like effector. Rather than a load at the end of a single line, a load handing in multiple lines will be more stable and provide more accuracy in e.g. geo-survey applications where the load could include ground-penetrating radar or sensitive instruments to measure magnetic field or gravity to be moved accurately as close to the ground as possible.

The general problem of cooperative load transport have been investigated in many papers, see e.g. [2], [3] and references therein. In most of these, external cameras are used to provide accurate positions of both the Unmanned Aerial Vehicles (UAVs) and payload, to be used in feedback control.

The use cases for this paper is aimed at out-door applications, where such external positional systems with the required accuracy and reliability may not always available. Instead, the hexacopters will be equipped with other sensors to measure their relative position to the load. Notable results for multi-lift systems with small-size helicopters have been reported by [4], [5] and [6]. In the latter, three helicopters autonomously transported a sensor-node equipped with a camera to the top of a building for aiding in a simulated search and rescue mission.

In our research, we are using the commercially available hexacopter from 3DRobotics [7]. The hexacopter is controlled by an autopilot called ArduPilot [8], which is an open-source autopilot, equipped with crucial flight components such as inertial measurement systems and communication links.

II. Contribution

The purpose of this paper is to derive a kinematic control law to guide a group of hexacopters to perform a transport maneuver of a suspended load. The chosen approach is to be used for a commercial hexacopter with autopilot, as seen in Figure 1. Our autopilot takes desired Euler angles and desired thrust as input signals.

Feedback to the kinematic controller is given by angle sensors, which measures the relative angle between the hexacopter and the load. The overall kinematic controller uses an approach that somewhat resembles the approach in [9], but in this paper we explicitly use available measurements from the angle sensor for feedback control.

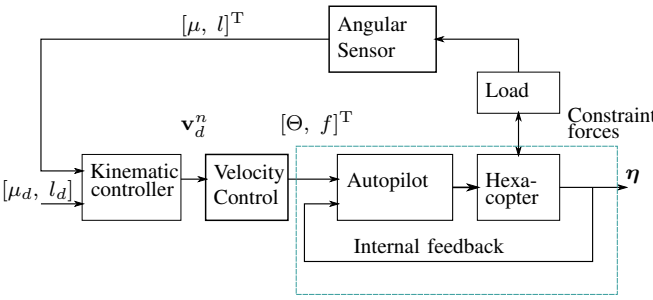

Fig. 1. Block diagram of the system. The boxes "autopilot" and "hexacopter" are commercially available systems. μ and l represents relative angle between the hexacopter and the suspended load. The velocity and kinematic controllers are discussed in VI and VII, respectively.

This work was partially supported by the Research Council of Norway through its Centers of Excellence funding scheme, project number 223254 (Centre for Autonomous Marine Operations and Systems).

A. Organization

First, in Section III, a model of a generic rigid body is presented, followed by some information about the hexacopter in Section IV. The Udwadia-Kalaba equation is introduced in Section V, along with definitions of the equations of constraints for the suspended-load system. In Section VI, a velocity controller for the hexacopter is designed. The proposed kinematic control law is presented in Section VII, followed by two simulations in Section VIII.

III. Rigid-Body Modelling

A. Kinematics

This section is a brief introduction to the nomenclature used extensively in the field of surface vessels and UAVs, as introduced by [10]. The NED frame, denoted $\{n\}$, is assumed inertial. Coordinates in this frame, denoted $\boldsymbol{\eta} \in \mathbb{R}^6$ are $[x^n \ y^n \ z^n \ \boldsymbol{\Theta}^{\mathrm{T}}]^{\mathrm{T}}$. $\boldsymbol{\Theta} = [\phi \ \theta \ \psi]^{\mathrm{T}}$ denotes the Euler-angles, as defined by the rotation sequence zyx [10]. The body-fixed coordinate system, denoted $\{b\}$, is attached to each rigid body. The body-velocities is given by

$$\boldsymbol{\nu} = \begin{bmatrix} u & v & w & p & q & r \end{bmatrix}^{\mathrm{T}} \tag{1}$$

where $\boldsymbol{\nu}_1 = [u, \ v, \ w]^{\mathrm{T}}$ and $\boldsymbol{\nu}_2 = [p, \ q, \ r]^{\mathrm{T}}$ refer to the translational and rotational motions, respectively, and likewise for $\boldsymbol{\eta}_1$ and $\boldsymbol{\eta}_2$. When working with kinematics, it is useful to define the following matrices [10]:

$$\mathbf{R}_b^n := \begin{bmatrix} c\psi c\theta & -s\psi c\phi + c\psi s\theta s\phi & s\psi s\phi + c\psi c\phi s\theta \\ s\psi c\theta & c\psi c\phi + s\phi s\theta s\psi & -c\psi s\phi + s\theta s\psi c\phi \\ -s\theta & c\theta s\phi & c\theta c\phi \end{bmatrix} \tag{2}$$

where $c\cdot = \cos(\cdot)$ and $s\cdot = \sin(\cdot)$. $\mathbf{R}_b^n$ is the rotation matrix describing the rotation of the frame $\{b\}$ relative to a frame $\{n\}$ subject the rotation $\boldsymbol{\Theta}$. Further,

$$\mathbf{S}(\lambda) := \begin{bmatrix} 0 & -\lambda_3 & \lambda_2 \\ \lambda_3 & 0 & -\lambda_1 \\ -\lambda_2 & \lambda_1 & 0 \end{bmatrix} \tag{3}$$

generates a skew symmetric matrix of $\lambda \in \mathbb{R}^3$ satisfying $\mathbf{S}(\lambda)^{\mathrm{T}} = -\mathbf{S}(\lambda)$ and $\lambda \times \lambda = \mathbf{S}(\lambda)\lambda$. Finally, let

$$\mathbf{T}_\Theta := \begin{bmatrix} 1 & s\phi s\theta/c\theta & c\phi s\theta/c\theta \\ 0 & c\phi & -s\phi \\ 0 & s\phi/c\theta & c\phi/c\theta \end{bmatrix}, \forall \theta \neq \frac{\pi}{2} + k\pi, k \in \mathbb{Z} \tag{4}$$

be the angular transformation matrix, relating angular speeds in $\{n\}$ and $\{b\}$ by $\dot{\boldsymbol{\Theta}} = \mathbf{T}_\Theta \boldsymbol{\nu}_2$

To summarize, velocities in $\{n\}$ and $\{b\}$ are related by

$$\dot{\boldsymbol{\eta}} = \mathbf{J}_\Theta \boldsymbol{\nu} \tag{5}$$

where

$$\mathbf{J}_\Theta = \begin{bmatrix} \mathbf{R}_b^n(\boldsymbol{\Theta}) & \mathbf{0}_{3\times3} \\ \mathbf{0}_{3\times3} & \mathbf{T}_\Theta \end{bmatrix} \tag{6}$$

as defined in [10].

B. Kinetics

The rigid-body kinetics of a generic body can be written [10]:

$$m(\dot{\boldsymbol{\nu}}_1 + \boldsymbol{\nu}_2 \times \boldsymbol{\nu}_1) = \boldsymbol{\tau}_1 \tag{7}$$

$$\mathbf{I}_{CG}\dot{\boldsymbol{\nu}}_2 + \boldsymbol{\nu}_2 \times (\mathbf{I}_{CG}\boldsymbol{\nu}_2) = \boldsymbol{\tau}_2 \tag{8}$$

where m is the mass of the body, $\mathbf{I}_{CG} \in \mathbb{R}^{3\times3}$ is the moment of inertia about the centre of gravity. $\boldsymbol{\tau}_1 \in \mathbb{R}^3$ is external forces and $\boldsymbol{\tau}_2 \in \mathbb{R}^3$ is external moments.

If one assume that $\{b\}$ is located in the centre of gravity, (7)–(8) can be rewritten to

$$\mathbf{M}\dot{\boldsymbol{\nu}} + \mathbf{C}(\boldsymbol{\nu})\boldsymbol{\nu} = \boldsymbol{\tau}_{RB} \tag{9}$$

where

$$\begin{aligned} \mathbf{M} &= \begin{bmatrix} m\mathbf{I}_{3\times3} & \mathbf{0}_{3\times3} \\ \mathbf{0}_{3\times3} & \mathbf{I}_{CG} \end{bmatrix}, \\ \mathbf{C}(\boldsymbol{\nu}) &= \begin{bmatrix} m\mathbf{S}(\boldsymbol{\nu}_2) & \mathbf{0}_{3\times3} \\ \mathbf{0}_{3\times3} & -\mathbf{S}(\mathbf{I}_{CG}\boldsymbol{\nu}_2) \end{bmatrix} \end{aligned} \tag{10}$$

Further, the gravitational forces acting on the body, $\mathbf{g}(\boldsymbol{\eta})$, can be written

$$\mathbf{g}(\boldsymbol{\eta}) = -\begin{bmatrix} (\mathbf{R}_b^n)^{\mathrm{T}}\mathbf{f}_G \\ \mathbf{0}_{3\times1} \end{bmatrix} \tag{11}$$

where $\mathbf{f}_G = [0 \ 0 \ mg]^{\mathrm{T}}$ is the gravitational force in $\{n\}$. The resulting model now becomes:

$$\dot{\boldsymbol{\eta}} = \mathbf{J}_\Theta \boldsymbol{\nu} \tag{12}$$

$$\mathbf{M}\dot{\boldsymbol{\nu}} + \mathbf{C}(\boldsymbol{\nu})\boldsymbol{\nu} + \mathbf{g}(\boldsymbol{\eta}) = \boldsymbol{\tau} \tag{13}$$

IV. Hexacopter dynamics

A multi-copter has the ability to individually control the moments $\boldsymbol{\tau}_2$ and the upwards thrust. Low-level control is covered in numerous articles, including for instance [11], [12] and [13].

Here we assume that the UAV is equipped with low-level controllers, allowing us to send desired Euler angles for roll, pitch and yaw as inputs. Additionally, the autopilot receives a control input $f \in [0 \dots 1]$ which sets the upwards thrust force. $f = 0.5$ represents a stable hovering hexacopter. The force F generated by $f = 0.5$ equals mg, thus $F = {}^{mg}/_{0.5} f := k_f f$.

In section VI, a controller for setting desired velocities in $\{n\}$ are designed.

V. Load Dynamics

In this section, a model of a slung-load system will be derived. This is based on the work of [1].

A suspended payload connected to n hexacopters with n wires produces a dynamical system with constraints given by the wire lengths. This behavior can be modeled by applying the principle of virtual work by D'Alembert using

a Lagrangian formulation [1]. But, as pointed out in [1], this leads to quite extensive modeling when a variable number of constraints must be handled.

Another way of dealing with constrained systems where introduced by Udwadia and Kalaba [14]. This method gives an explicit equation for additional forces acting on the constrained bodies, and thus makes it simple to utilize for different configurations. Notice that the equations of Udwadia-Kalaba and Lagrange are equivalent, as shown in [15].

A. The Udwadia-Kalaba equation

This section follows the derivation in [1]. Consider the unconstrained Newtonian system

$$\mathbf{M}\ddot{\mathbf{q}}_u = \mathbf{Q} \tag{14}$$

where $\mathbf{q}_u \in \mathbb{R}^{n_q}$ is the unconstrained generalized coordinates of the system, and $\mathbf{Q} \in \mathbb{R}^{n_q}$ are generalized forces. Now, let the system be subjected to n constraints in the form

$$\mathbf{A}(\mathbf{q}, \dot{\mathbf{q}}, t)\ddot{\mathbf{q}} = \mathbf{b}(\mathbf{q}, \dot{\mathbf{q}}, t) \tag{15}$$

where $\mathbf{A} \in \mathbb{R}^{n \times n_q}$ and $\mathbf{b} \in \mathbb{R}^n$ and $\mathbf{q}$ the generalized coordinates of the constrained motion of (14).

The system (14) can be transformed to a constrained system by augmenting it with a constraint force $\mathbf{Q}_c \in \mathbb{R}^{n_q}$ as:

$$\mathbf{M}\ddot{\mathbf{q}} = \mathbf{Q} + \mathbf{Q}_c \tag{16}$$

In [14], (16) is solved by applying Gauss's principle of Least Constraints. This principle states that the acceleration of the constrained system follows the vector closest to the unconstrained acceleration, that satisfies the constraints. This leads to a minimization problem, which can be solved using the Moore-Penrose pseudoinverse. Moreover, the constrained system's acceleration $\ddot{\mathbf{q}}$ can be found from (see [1] and [14]):

$$\ddot{\mathbf{q}} = \ddot{\mathbf{q}}_u + \mathbf{M}^{-1/2}(\mathbf{A}\mathbf{M}^{-1/2})^{+}(\mathbf{b} - \mathbf{A}\ddot{\mathbf{q}}_u) \tag{17}$$

where $(\cdot)^{+}$ denotes the Moore-Penrose pseudoinverse. This makes it possible to explicitly identify the constraint force $\mathbf{Q}_c$ as

$$\mathbf{Q}_c = \mathbf{M}^{1/2}(\mathbf{A}\mathbf{M}^{-1/2})^{+}(\mathbf{b} - \mathbf{A}\ddot{\mathbf{q}}_u) \tag{18}$$

B. Equations of constraint for the suspended load

The next step is to develop equations for the constraints in the form $\mathbf{A}\ddot{\mathbf{q}} = \mathbf{b}$. Let wire j be attached to CG of hexacopter j, and connected to the load CG. In the rest of this paper, the subscript $(\cdot)_j$ denotes element $(\cdot)$ for hexacopter j. The vector from the load to hexacopter j is:

$$\mathbf{L}_j^n = \boldsymbol{\eta}_j - \boldsymbol{\eta}_l \tag{19}$$

Let the constraint equation be chosen as

$$g_j = ||\mathbf{L}_j^n||^2 - d_j^2 \tag{20}$$

where d_j is the length of wire j. It is desired to express the resulting equations in $\{b\}$, so let the generalized acceleration vector $\ddot{\mathbf{q}}$ be:

$$\ddot{\mathbf{q}} = \begin{bmatrix} \dot{\boldsymbol{\nu}}_1 & \dot{\boldsymbol{\nu}}_2 & \dot{\boldsymbol{\nu}}_j & \cdots & \dot{\boldsymbol{\nu}}_m & \dot{\boldsymbol{\nu}}_l \end{bmatrix}^{\mathrm{T}} \tag{21}$$

Then,

$$\frac{\mathrm{d}^2}{\mathrm{d}t^2} g_j = 2(\mathbf{L}_j^n)^{\mathrm{T}}(\mathbf{R}_{b,j}^n \dot{\boldsymbol{\nu}}_j - \mathbf{R}_l^n \dot{\boldsymbol{\nu}}_l) + 2\dot{\mathbf{L}}_j^{\mathrm{T}} \dot{\mathbf{L}}_j \tag{22}$$

and we can recognize $\mathbf{A}_j$ and b_j as

$$\mathbf{A}_j = 2(\mathbf{L}^n)^{\mathrm{T}} \begin{bmatrix} \mathbf{0}_{3\times 6(j-1)} & \mathbf{R}_{b,j}^n & \mathbf{0}_{3\times 3} & \cdots \\ & \mathbf{0}_{3\times 6(m-j)} & -\mathbf{R}_l^n & \mathbf{0}_{3\times 3} \end{bmatrix} \tag{23}$$

$$b_j = -2\dot{\mathbf{L}}_j^{\mathrm{T}} \dot{\mathbf{L}}_j \tag{24}$$

We can now calculate the constrained accelerations from (17).

C. Simulation and numerical considerations

The equations of constraints developed here, ensures that the second-order derivative of g_j equals 0. However, due to numerical error in when integrating, $g_j = 0$ will generally not be achieved. This will make the length of the wires drift, and is a well recognized problem in the litterature [16]. As discussed in [1], several approaches to counter this problem exists. [1] evaluates two approaches, and yields good results by applying a virtual spring-damper approach. Here, a virtual spring-damper system is added along all wires to ensure that $g_j = 0$. Further details can be found in [1] and [17].

VI. Velocity Control Design

As discussed in Section IV, the hexacopter autopilot takes the Euler angles $\boldsymbol{\Theta}$ and a thrust force f as input. The translational force in $\{n\}$ generated from the hexacopter propellers are given by

$$\boldsymbol{\tau}^n = \mathbf{R}_b^n \begin{bmatrix} 0 \\ 0 \\ -F \end{bmatrix} \tag{25}$$

where $F = k_f f$. This can be expanded to:

$$\tau_x^n = -k_f f(\sin\psi \sin\phi + \cos\psi \cos\phi \sin\theta) \tag{26}$$

$$\tau_y^n = -k_f f(-\cos\psi \sin\phi + \sin\theta \sin\psi \cos\phi) \tag{27}$$

$$\tau_z^n = -k_f f(\cos\theta \cos\phi) \tag{28}$$

By using (26)–(28), Algorithm 1 summarizes how to generate desired angles based on a desired force in $\{n\}$.

Algorithm 1 (Generation of translational forces)**.** *Given desired force $\mathbf{F}_d^n \in \mathbb{R}^3$ to be applied by the motors. Let ϕ, θ, and ψ be current roll, pitch and yaw angle, respectively. The goal is to create desired angles ϕ_d, θ_d and ψ_d to realize the desired force.*

1) *Using* (28)*, set $f = -F_{d,z}^n/(k_f \cos\theta \cos\phi)$ to gain upwards thrust and compensate for hexacopter tilt.*

2) Using the current yaw angle ψ and F from Step 1, (26)–(27) *becomes a set of two equations with two unknowns. Setting $\psi_d = 0$, gives*

$$\tau_x^n = -k_f f(\cos\phi_d \sin\theta_d) \tag{29}$$

$$\tau_y^n = k_f f(\sin\phi_d) \tag{30}$$

which can be solved for ϕ_d and θ_d.

Further, by the parameterization of $\mathbf{C}(\boldsymbol{\nu})$ in Section III, it can be shown that the translational motion in $\{n\}$ can be written as:

$$m\dot{\mathbf{v}}^n = \mathbf{F}_g^n + \mathbf{F}_l^n + \boldsymbol{\tau}^n \tag{31}$$

where $\mathbf{F}_l^n$ and $\mathbf{F}_g^n$ is pull by gravity and the load. The load disturbs the motion of the helicopter with a force $|F_l|$ pointed along the wire. The direction of the wire is represented by the angles $[\mu,\ l]^{\mathrm{T}}$, which is defined by Figure 2. The components of this force can be calculated as

$$\mathbf{F}_l^n = \begin{bmatrix} F_{l,x} \\ F_{l,y} \\ F_{l,z} \end{bmatrix} = \begin{bmatrix} -|F_l|\cos l \cos\mu \\ -|F_l|\sin l \cos\mu \\ |F_l|\sin\mu \end{bmatrix} \tag{32}$$

The pull from the suspended laod needs to be compensated for, in addition to gravity. Let the desired thrust in $\{n\}$ be:

$$\boldsymbol{\tau}^n = -\mathbf{F}_g^n - \mathbf{F}_l^n + \boldsymbol{\alpha} \tag{33}$$

where $\boldsymbol{\alpha}$ is an additional control force to be designed. Given reference velocities $\mathbf{v}_d^n$ in $\{n\}$, we propose the following control law:

Theorem 1. *Given a desired velocity $\mathbf{v}_d^n$, the controller*

$$\boldsymbol{\alpha} = m\dot{\mathbf{v}}_d^n + \mathbf{K_p}(\mathbf{v}_d^n - \mathbf{R}_b^n\boldsymbol{\nu}_1) + \mathbf{K_d}(\dot{\mathbf{v}}_d^n - \mathbf{R}_b^n(\mathbf{S}(\boldsymbol{\nu}_2)\boldsymbol{\nu}_1 + \dot{\boldsymbol{\nu}}_1)) \tag{34}$$

where $\mathbf{K}_k \in \mathbb{R}^{3\times3} = \mathbf{K}_k > 0, k \in \{p, d\}$ will render the equilibrium point $\mathbf{v}^n = \mathbf{v}_d^n$ of (31) *exponentially stable (GES).*

Proof: Let $\tilde{\mathbf{v}} := \mathbf{v}^n - \mathbf{v}_d^n$. By using $\boldsymbol{\nu}_1 = (\mathbf{R}_b^n)^{\mathrm{T}}\dot{\boldsymbol{\eta}}_1$ and $\dot{\boldsymbol{\nu}}_1 = (\dot{\mathbf{R}}_b^n)^{\mathrm{T}}\dot{\boldsymbol{\eta}} + (\mathbf{R}_b^n)^{\mathrm{T}}\ddot{\boldsymbol{\eta}}_1$, inserting into (34) yields:

$$\boldsymbol{\alpha} = m\dot{\mathbf{v}}_d^n - \mathbf{K_p}\tilde{\mathbf{v}} - \mathbf{K_d}\dot{\tilde{\mathbf{v}}}$$

By using (31), we get

$$\dot{\tilde{\mathbf{v}}} = -(m\mathbf{I} + \mathbf{K}_d)^{-1}\mathbf{K}_p\tilde{\mathbf{v}}$$

which proves that the zero-equilibrium $\tilde{\mathbf{v}} = 0$ is GES. ∎

VII. Group Coordination

Let the position of hexacopter j relative to the load be expressed in the spherical coordinates $\begin{bmatrix} l_j, & \mu_j, & d_j \end{bmatrix}$, as described in Figure 2. Then, the desired velocity calculated from the following controller will bring the system into a desired configuration:

Theorem 2. *Let $l_d \in \mathbb{R}^m$ be evenly distributed in $(-\pi \ldots \pi]$. Given desired configuration angle μ_d, n hexacopters will evenly distribute themselves with the kinematic control law*

$$\mathbf{v}_{d,j}^n = \mathbf{R}_{l,j}^n \begin{bmatrix} k_1(\mu_{d,j} - \mu_j) & -k_2(l_{d,j} - l_j) & 0 \end{bmatrix}^{\mathrm{T}} \tag{35}$$

Proof: Let there be a coordinate frame $\{l_j\}$ centered in hexacopter j, which is rotated such that $z^{l,j}$ points towards the suspended load, $y^{l,j}$ is directed along $z^{l,j} \times z^n$, and $x^{l,j}$ completes the right-hand rule (see Figure 2). Let $u^{l,j},\ v^{l,j},\ w^{l,j}$ be linear velocities along $x^{l,j},\ y^{l,j},\ z^{l,j}$, respectively.

A coordinate transformation between $\{l_j\}$ and $\{n\}$ is given by a principal rotation $\pi + l_j$ over the z^n-axis, followed by a rotation $\pi/2 - \mu_j$ over the y^n-axis [10].

$$\begin{aligned} \mathbf{R}_{l,j}^n &= \mathbf{R}_{z,\pi+l_j}\mathbf{R}_{y,\frac{\pi}{2}-\mu_j} \\ &= \begin{bmatrix} -\cos l_j \sin\mu_j & \sin l_j & -\cos l_j \cos\mu_j \\ -\sin l_j \sin\mu_j & -\cos l_j & -\sin l_j \cos\mu_j \\ -\cos\mu_j & 0 & \sin\mu_j \end{bmatrix} \end{aligned} \tag{36}$$

From the definition of $\{l_j\}$, we have

$$\dot{\mu}_j = du^{l,j}$$

$$\dot{l}_j = -dv^{l,j}$$

Let $\tilde{(\cdot)} := (\cdot)_d - (\cdot)$. Then, by $u^{l,j} = k_1\tilde{\mu}_j$ and $v^{l,j} = -k_2\tilde{l}_j$:

$$\dot{\tilde{\mu}}_j = -dk_1\tilde{\mu}_j \tag{37}$$

$$\dot{\tilde{l}}_j = -dk_2\tilde{l}_j \tag{38}$$

which makes the zero-equilibrium points in (37)–(38) exponentially stable. Set $\mathbf{v}_{d,j}^{l,j} = [u^{l,j},\ v^{l,j},\ 0]^{\mathrm{T}}$. Then, the reference velocity in $\{n\}$ is given by

$$\mathbf{v}_{d,j}^n = \mathbf{R}_{l,j}^n\mathbf{v}_{d,j}^{l,j} \tag{39}$$

∎

The desired velocity $\mathbf{v}_{d,j}^n$ gained from (35) is then used together with (34) to generate a desired thrust for each hexacopter. The angles μ_j and l_j can be measured by first measuring angles relative to $\{b\}$ by on-board angular sensors, and supplying with information in $\boldsymbol{\Theta}$. More specifically, l_j requires knowledge of the heading ψ, while μ_j requires the current roll ϕ and pitch θ angles.

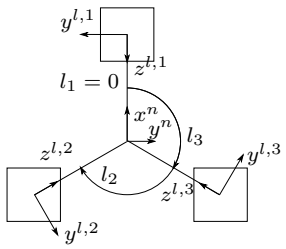

(a) Top view. Three hexacopters are positioned evenly around a load in the center.

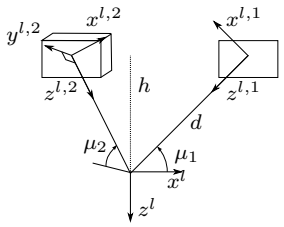

(b) Side view where you can see two hexacopter bodies and their relative position to the load.

Fig. 2. Illustration of the l-frame.

VIII. Simulation Study

A. Simulation 1: Formation stabilization

In this section a simulation with three identical hexacopters will be conducted. The three hexacopters are connected to

a load with three ropes, assumed massless. The system is modelled using the results in Section V. Each hexacopter has a mass of 4 kg, while the load weights 0.5 kg. The ropes are connected to the CG of both the load and the hexacopters. The autopilot is simulated with a PD-type controller width a bandwidth of 5 rad/s. The controller also has a maximum value for the roll and pitch angles set to 15° to ensure smooth flights.

The load is initially placed at $[0, 0, 0]^{\mathrm{T}}$, while the hexacopters are placed around the load, each with a distance of $d_j = 2$, with the following coordinates:

$$\begin{bmatrix}\mu_1\\ l_1\end{bmatrix} = \begin{bmatrix}30^\circ\\ -180^\circ\end{bmatrix}, \quad \begin{bmatrix}\mu_2\\ l_2\end{bmatrix} = \begin{bmatrix}45^\circ\\ -60^\circ\end{bmatrix}, \quad \begin{bmatrix}\mu_3\\ l_3\end{bmatrix} = \begin{bmatrix}60^\circ\\ 60^\circ\end{bmatrix}$$

The desired μ_d for all hexacopters are $\mu_d = 45^\circ$. Further, the desired l_ds are

$$l_{d,1} = -120^\circ, \quad l_{d,2} = 0^\circ, \quad l_{d,3} = 120^\circ$$

The numerical integration is done with Runge-Kutta 4, running at 100 Hz. The results can bee seen in Figures 3–5.

In the simulations, the variables μ and l must be calculated from the current position of the load and each hexacopter. Let $\bar{\mathbf{x}}_j = [\bar{x}_j,\ \bar{y}_j,\ \bar{z}_j] := \eta_j - \eta_l$. Then, μ_j and l_j can be calculated by:

$$\mu_j = \operatorname{atan}\left(\frac{-\bar{z}_j}{\sqrt{\bar{x}_j^2 + \bar{y}_j^2}}\right) \tag{40}$$

$$l_j = \operatorname{atan2}(\bar{y}_j, \bar{x}_j) \tag{41}$$

which is valid for $\bar{x}_j^2 + \bar{y}_j^2 \neq 0$, that is, when the load is not directly above or below a hexacopter.

B. Results and discussions

Figure 3 shows the time plot of μ and l for all three hexacopters. It it seen that the controller forces μ_j and l_j to their desired values. Further, the constrained acceleration of the load can be seen in Figure 4(a). It is seen that after the hexacopters reach their position, they stabilize the position of the load. But, as can be seen by Figure 4(b), the position of the load drifts a bit while they get into formation. This is due to the fact that no attempt to control the position of the load is done in this simulation. This is done in the next section.

Further, the roll and pitch of hexacopter 1 can be seen in Figure 5. It can be seen that the stationary value is not zero, indicating that the hexacopter must be tilted to compensate for the additional pull from the load-wire.

C. Simulation 2: Load transport

The start of this simulation is identical to that of the previous section, but here, after a stable formation is reached, an additional velocity component is inserted to transport the load to a desired location. Let $\boldsymbol{\eta}_{l,d} \in \mathbb{R}^3$ be the desired position of the load. Further, let $\mathbf{v}_{d,p}^n \in \mathbb{R}^3$ be the velocity component to guide the load to its desired position, be

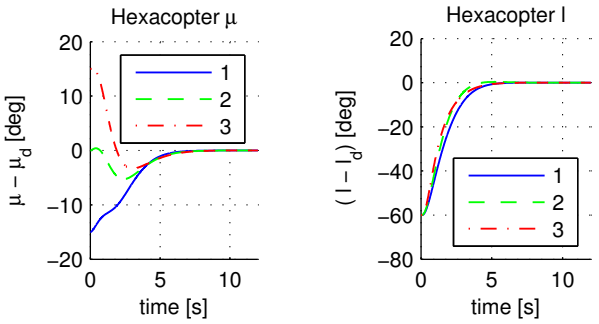

(a) Error in μ for hexacopter 1-3 (in degrees).

(b) Error in l for hexacopter 1-3 (in degrees).

Fig. 3. μ and l for all hexacopters. In both 3(a) and 3(b), the blue line is for hexacopter 1, the dashed green for hexacopter 2, and the dash-dotted line for hexacopter 3.

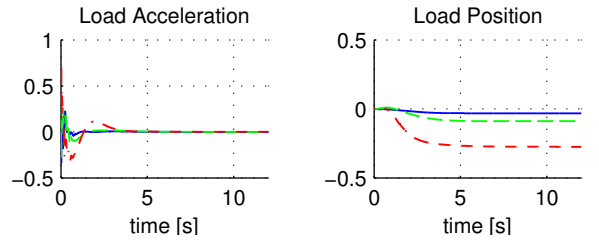

(a) Load constrained acceleration.

(b) Load position. It is seen that the position drifts a bit from the initial position.

Fig. 4. Load acceleration (4(a)) and position (4(b)). In both figures, blue, green and red represents the directions x^n, y^n and z^n, respectively.

$$\mathbf{v}_{d,p}^n = K_l(\boldsymbol{\eta}_{l,d} - \boldsymbol{\eta}_l)$$

so that after the desired configuration is reached, the total reference velocity is $\mathbf{v}_{d,p}^n + \mathbf{v}_{d,j}^n$, where the last term is calculated from (39). In this simulation, $\boldsymbol{\eta}_{l,d} = [1,\ 5,\ 0]^{\mathrm{T}}$ and $K_l = 1$. The results of the simulation can be seen in Figures 6–9.

D. Results and discussions

In Figure 6, it is seen that the error in μ_j and l_j stays at zero during the transport manoeuvre, which shows the feasibility of the proposed controller. Further, Figure 7(b) shows that the load is transported to the desired location $[1,\ 5,\ 0]^{\mathrm{T}}$. From Figure 8, it is seen that the velocity-controller for hexacopter 1 follows the desired velocities. A time-lapse of the maneuver can be seen in Figure 9, at the times indicated in the figure.

IX. Conclusions

We have derived a nonlinear kinematic control law for cooperative load transport using multiple hexacopters. The proposed control law can be used as a guidance law for a hexacopter with autopilot. Numerical simulations verify the results.

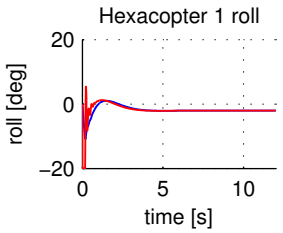

(a) Roll (blue) and reference for hexacopter 1.

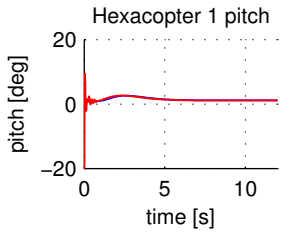

(b) Pitch (blue) and reference for hexacopter 1.

Fig. 5. Roll (5(a)) and pitch (5(b)) for hexacopter 1.

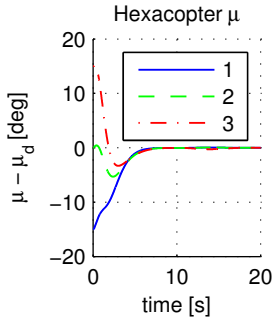

(a) Simulation 2: Error in μ for hexacopter 1-3 (in degrees).

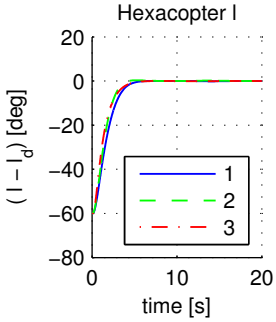

(b) Simulation 2: Error in l for hexacopter 1-3 (in degrees).

Fig. 6. μ and l for all hexacopters in Simulation 2. In both 6(a) and 6(b), the blue line is for hexacopter 1, the dashed green for hexacopter 2, and the dash-dotted line for hexacopter 3.

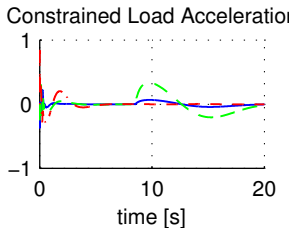

(a) Simulation 2: Load constrained acceleration.

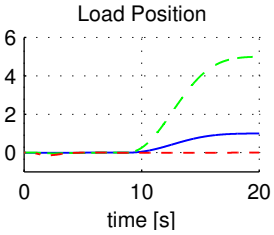

(b) Simulation 2: Load position. It is seen that the position drifts a bit from the initial position.

Fig. 7. Simulation 2: Load acceleration (7(a)) and position (7(b)). In both figures, blue, green and red represents the directions x^n, y^n and z^n, respectively.

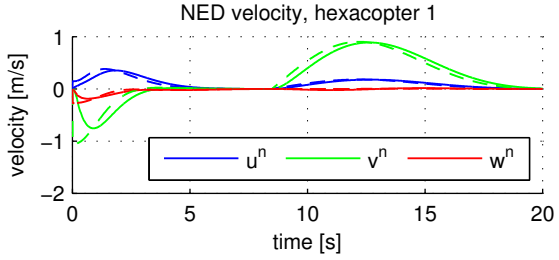

Fig. 8. Simulation 2: Simulation ned velocity for hexacopter 1.

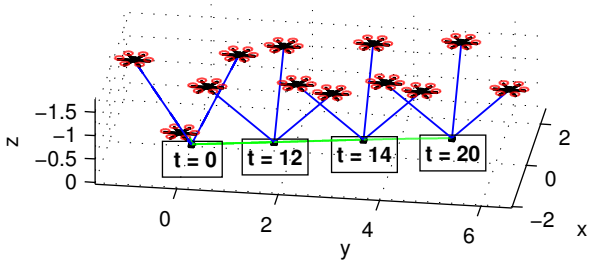

Fig. 9. Simulation 2: Trajectory overview.

REFERENCES

[1] M. Bisgaard, "Modeling, Estimation, and Control of Helicopter Slung Load System," Ph.D. dissertation, Aalborg University, 2008.

[2] D. Mellinger, M. Shomin, N. Michael, and V. Kumar, "Cooperative grasping and transport using multiple quadrotors," *Distributed autonomous robotic systems autonomous robotic systems*, pp. 545–558, 2013.

[3] N. Michael, J. Fink, and V. Kumar, "Cooperative manipulation and transportation with aerial robots," *Autonomous Robots*, vol. 30, no. 1, pp. 73–86, Sept. 2010.

[4] I. Maza, K. Kondak, M. Bernard, and a. Ollero, "Multi-UAV Cooperation and Control for Load Transportation and Deployment," *Journal of Intelligent and Robotic Systems*, vol. 57, no. 1-4, pp. 417–449, Aug. 2009.

[5] M. Bernard and K. Kondak, "Generic slung load transportation system using small size helicopters," *2009 IEEE International Conference on Robotics and Automation*, pp. 3258–3264, May 2009.

[6] ——, "Autonomous transportation and deployment with aerial robots for search and rescue missions," *Journal of Field Robotics*, vol. 28, no. 6, pp. 914–931, 2011.

[7] 3DRobotics, "http://3drobotics.com."

[8] Ardupilot, "http://ardupilot.com."

[9] T. Lee, K. Sreenath, and V. Kumar, "Geometric Control of Cooperating Multiple Quadrotor UAVs with a Suspended Payload," *cmu.edu*, pp. 5510–5515, 2013.

[10] T. I. Fossen, *Marine Craft Hydrodynamics and Motion Control*. Wiley, 2011.

[11] A. Alaimo, V. Artale, C. Milazzo, A. Ricciardello, and L. Trefiletti, "Mathematical modeling and control of a hexacopter," in *2013 International Conference on Unmanned Aircraft Systems (ICUAS)*. Ieee, May 2013, pp. 1043–1050.

[12] M. Hehn and R. D'Andrea, "Quadrocopter trajectory generation and control," in *IFAC World Congress*, 2011.

[13] R. Mahony, V. Kumar, and P. Corke, "Modeling, Estimation, and Control of Quadrotor," *IEEE Robotics & Automation magazine*, no. September, pp. 20–32, Sept. 2012.

[14] F. Udwadia and R. Kalaba, "A new perspective on constrained motion," *Proceedings: Mathematical and Physical Sciences*, vol. 439, no. 2, pp. 407–410, 1992.

[15] F. E. Udwadia, "Equations of motion for mechanical systems: A unified approach," *Journal of Non-linear Mechanics*, vol. 31, no. 6, pp. 951–958, 1996.

[16] M. Cline and D. Pai, "Post-Stabilization for Rigid Body Sim- ulation with Contact and Constraints," *Proceedings of the IEEE International Conference on Robotics and Automation, 2003.*, vol. 3, no. 1, pp. 3744–3751, 2003.

[17] M. Bisgaard, J. D. Bendtsen, and A. L. Cour-Harbo, "Modeling of Generic Slung Load System," *Journal of Guidance, Control, and Dynamics*, vol. 32, no. 2, pp. 573–585, Mar. 2009.